

ARTICLES

Cryogenic Transmission Electron Microscopy (Cryo-TEM) of Micelles and Vesicles Formed in Water by Poly(ethylene oxide)-Based Block Copolymers

You-Yeon Won,[†] Aaron K. Brannan, H. Ted Davis, and Frank S. Bates*Department of Chemical Engineering and Materials Science, University of Minnesota,
Minneapolis, Minnesota 55455

Received: September 27, 2001; In Final Form: January 3, 2002

We investigated the micellar polymorphism of poly(ethylene oxide)(PEO)-based block copolymers to illustrate the possibility of a rational control of the aggregation structure through synthetic manipulation of the molecular characteristics. Boundaries for the micellar shape transitions from bilayers to cylinders to spheres with increasing PEO composition were determined with direct cryogenic transmission electron microscopic (cryo-TEM) imaging of the microstructures in the form of thin vitreous hydrated specimens. Analyses of cryo-TEM images lead to determination of the packing properties of the hydrophobic block in terms of the interfacial area per chain and the degree of chain stretching. Also, the micellar phases of the block copolymers are characterized by anomalous structural behaviors such as coexistence of different structures and formation of exotic compound structures, which are discussed in terms of metastability inherent in the system comprising polymeric materials.

Introduction

Amphiphilic block copolymers are macromolecules consisting of one or more hydrophilic blocks covalently connected to a series of hydrophobic blocks. This class of block copolymers is now recognized as an excellent macromolecular counterpart to conventional amphiphilic materials such as surfactants and lipids with greater availability of chemical identities and molecular characteristics. When dispersed in selective solvents (that is, those miscible with one but not with the other, say water), these materials self-assemble to create dispersed microphases, with the hydrophobic chains sequestering themselves into microdomains of a certain shape and the hydrophilic chains orienting themselves toward the aqueous phase. Particularly in the dilute limit, discrete supramolecular aggregates such as globular or extended micelles or vesicles (i.e., bilayered membrane bags) are formed.^{1–4} The size, shape, and state of dispersion of these microscopic association colloids are dictated by the molecular size, composition, and architecture, and the concentration of the amphiphile. Understanding the connection between supramolecular microstructure and molecular structure is essential for a wide range of technical applications in which the desired function of a complex fluid is made possible through the precise control of the self-assembled microstructure. Well-known examples include vesicles for biological cell imitation or drug delivery⁵ and the long cylindrical micelles for drag reduction.⁶

Elegant phenomenological (i.e., semiempirical) considerations^{7,8} have been advanced to explain the observed correlation between the optimal aggregation geometry among the three basic choices (i.e., sphere, cylinder, and bilayer) and the molecular

characteristics of the amphiphiles, providing useful, albeit qualitative, insights into the mechanisms of amphiphilic association. Those models rationalize the preferred geometries in terms of the ratio between the measured interfacial area per chain (a_0) and the cross-sectional area of the hydrophobic chain (v/l_c , where v and l_c are the volume and length of the hydrophobic chain, respectively). In fact, the optimal headgroup area per chain is determined through a competition among interfacial tension, headgroup repulsion, and entropic penalty for hydrophobic chain deformation, and theories are able to qualitatively model this competition and predict the sequence of microstructures^{9–13}. In regards to the aggregation behavior of block copolymers in dilute solutions, it is reasonable to expect that greater entropic (configurational) degrees of freedom associated with the high molecular weight^{14,15} further confound attempts to address the issue of the mechanisms of selection of the optimal geometries. A great deal of research activity has focused on the study of the structural properties of the solvated polymer chains (that is, *polymer brushes*) attached to the surface the geometry of which is normally given as an input.^{16–21}

There are few research groups that have reported direct visualization of polymeric aggregates in water. Zhang and Eisenberg first showed multiple nonspherical micelle-like morphologies formed by hydrated poly(acrylic acid)–polystyrene (PAA–PS) using regular transmission electron microscopy (TEM).¹ Eisenberg and co-workers' subsequent experiments to date represent a rare experimental effort that in a comprehensive manner addresses the issue of how the aggregation structure can be rationally controlled through changes in molecular parameters utilizing amphiphilic block copolymers. Their approach for creating the *crew-cut* aggregates (that is, the corona size is smaller than the core size) made up of poly(ethylene oxide)–polystyrene (PEO–PS),^{22–25} PAA–PS,^{1,23,26,27} or poly-

* To whom correspondence should be addressed.

[†] Present address: Department of Materials Science and Engineering, Massachusetts Institute of Technology, Cambridge, MA 02139.

(acrylic acid)–polybutadiene (PAA–PB)²⁸ is to dissolve the copolymer in a common solvent, often dimethylformamide (DMF), and then to add water to induce reversible association of the hydrophobic segments. A transition between spheres and rods and bilayers can be induced by increasing the hydrophilic composition, and a spectrum of exotic compound structures have been identified in the crew-cut aggregate systems. Although their experimental path taken for creating the microphase separation is optimal for such highly asymmetric block copolymers with low hydrophilic content, such methods favor nonequilibrium structures through kinetic fixation and therefore may not be ideal for probing the aqueous aggregation behavior of polymeric amphiphiles from an equilibrium perspective.

This paper investigates the morphological properties of micelles and vesicles prepared from various PEO-based block copolymers by utilizing cryogenic transmission electron microscopy (cryo-TEM) as a major technique. The materials chosen for the hydrophobic cores are low molecular weight poly(1,2-butadiene) (1,2-PB as shorthand) and its saturated analogue poly(ethyl ethylene) (PEE). The glass transition temperatures (T_g) are $-12\text{ }^\circ\text{C}$ for 1,2-PB²⁹ and $-20\text{ }^\circ\text{C}$ for PEE,³⁰ and the entanglement molecular weights (M_e) are 2.0 kg/mol for 1,2-PB^{31,32} and 9.5 kg/mol for PEE.³² Therefore, unwanted coupling between the structural equilibration of the aggregates prepared from dry bulk polymer and glassy or entanglement dynamics of the core domain is highly unlikely to complicate our experiments.

The cryo-TEM technique is uniquely suited for identifying the local microstructures in complex fluids at high water content such as micellar and vesicular dispersions. In dealing with surfactant or lipid aggregations that are normally several nanometers in cross-sectional dimension, the structural measurements performed with cryo-TEM hardly provide quantitative information because the typical resolution that results from the phase contrast imaging is roughly on the same order of the size of the objects being probed. When used for polymeric aggregates the size of which is nearly an order of magnitude greater, cryo-TEM is a good quantitative probe that does not require any model-dependent analysis. In this paper, on the basis of the structural measurements using cryo-TEM, we establish the connection between the molecular composition and the morphology of the aggregation formed in water by the self-assembly of the polymeric amphiphiles and also the packing properties of the molecules.

Experimental Section

Materials. Eleven PEO-based di- and triblock copolymers used for this study were synthesized using techniques described elsewhere.^{33,34} Mono- or dihydroxyl end-functionalized poly(1,2-butadiene) was anionically polymerized with lithium or potassium counterion in tetrahydrofuran (THF). The PB precursor was converted to PEE by palladium-catalyzed hydrogenation to complete saturation. Ethylene oxide (EO) units were subsequently added to the pristine (PB) or hydrogenated (PEE) precursor, using potassium naphthalenide, to form the PEO block. The polydispersity index (PDI) was determined by gel permeation chromatography (GPC) using a Waters 150C differential refractometer fitted with Phenogel columns on the basis of a standard PS (Pressure Chemical Co) calibration. ¹H NMR was used to determine the molecular characteristics including the microstructure of the PB precursor (i.e., 1,2-addition %). The number-average molecular weight (M_n) and the melt volume fraction of PEO (f_{EO}) were calculated from the reaction stoichiometry using the amorphous densities

TABLE 1: Packing Characteristics of the Polymeric Aggregates

polymer	N_{core}^a	morphology	R_c^b (nm)	a_o^c (nm ²)	s^d
OB1	46	S	9.1	1.6	2.4
OB2	46	B	4.8	1.0	1.2
OB3	46	C	7.7	1.2	2.0
OE7	37	B	4.0	1.0	1.2
		C	5.7	1.4	1.7
OE8	35	C	5.1	1.5	1.6
		B	3.4	1.1	1.0
OEO1	42	C	6.8	1.3	1.8
		S	10.2	1.3	2.7
OEO10	38	C	6.3	1.3	1.8
		B	4.0	1.0	1.1
		S	9.1	1.3	2.6

^a Number of hydrophobic repeat units: $N_{\text{PB}} + 1$ for OBs; $N_{\text{PEE}} + 1$ for OEs; $N_{\text{PEE}}/2$ for OEOs. ^b Core domain size; radius for spheres (S) and cylinders (C), and half-thickness for bilayered vesicles (B). ^c Interfacial area per chain. ^d Degree of hydrophobic chain stretching defined as $s \equiv R_c/\langle r^2 \rangle_o^{1/2}$ where $\langle r^2 \rangle_o^{1/2}$ is the end-to-end distance of the hydrophobic chain in the random-walk configuration.

TABLE 2: Molecular Characteristics of the Block Copolymers

sample ID	chemical identity	M_n (kg/mol)	f_{EO}	PDI	structures ^a
OB1	PEO–PB	8.1	0.66	1.13	S
OB2	PEO–PB	3.6	0.28	1.13	B
OB3	PEO–PB	4.9	0.45	1.09	C
OB6	PEO–PB	13.1	0.52	1.09	C, S
OB12	PEO–PB	5.3	0.49	1.10	C
OE4	PEO–PEE	4.3	0.44	1.09	C, B
OE7	PEO–PEE	3.9	0.39	1.10	B, C
OE8	PEO–PEE	3.9	0.42	1.09	C, B
OEO1	PEO–PEE–PEO	11.2	0.53	1.11	C, S
OEO3	PEO–PEE–PEO	2.9	0.51	1.22	C, S
OEO10	PEO–PEE–PEO	8.4	0.44	1.17	C, B, S

^a Aggregation morphologies formed in water identified with cryo-TEM: B = bilayered vesicle; C = cylinder; S = sphere. Coexisting structures are written in the order of predominance.

estimated from published data for hydrogenous PB, PEE, and PEO at room temperature³² (i.e., $\rho_{90\%1,2\text{-PB}} = \rho_{\text{PEE}} = 0.87\text{ g/cm}^3$, and $\rho_{\text{PEO}} = 1.13\text{ g/cm}^3$). The molecular characteristics and also the resulting morphologies formed in water identified by cryo-TEM are summarized in Table 2.

One percent (by weight) solutions of the pure block copolymers were prepared by adding pure water (HPLC grade, Aldrich) directly into the weighed amount of dry bulk polymer. Then the sample was sealed and stirred at room temperature with a magnetic stirring bar rotating at several hertz until complete dissolution. All of the solution samples were equilibrated for at least 5 days, and the morphological characterization was carried out after the polymers were completely dispersed without any macroscopic heterogeneity in the sample judged by the naked eye.

Cryogenic Transmission Electron Microscopy. Cryo-TEM samples were prepared utilizing a custom-built chamber often referred to as the controlled environment vitrification system (CEVS).^{35,38} To prevent any water evaporation from the sample, the isolated chamber was humidified to near saturation of water before the sample was introduced. All of the samples were prepared at room temperature ($23 \pm 0.5\text{ }^\circ\text{C}$). In the CEVS, the sample in the form of a $\sim 5\text{-}\mu\text{L}$ droplet was placed on a microperforated cryo-TEM grid. It was then soaked by a filter paper, resulting in the formation of thin liquid films of 10–300 nm thickness freely spanning across the micropores in a carbon-coated lacelike polymer layer supported by a meshy metal grid. After a minimum 30-s detainment, the sample grid assembly was rapidly vitrified with liquid ethane at its melting

temperature (~ 90 K). The delay was adopted to relax any possible flow deformation that may have resulted from the blotting process. The vitreous specimen was kept under liquid nitrogen until it was loaded into a cryogenic sample holder (Gatan 626). Imaging was performed with a JEOL 1210 operating at 120 kV. The use of a minimal dose system (MDS) was necessitated by the electron radiation sensitivity of the sample probed. Adequate phase contrast was obtained at a nominal underfocus of 3–26 μm . Images were recorded on a Gatan 724 multiscan digital camera and processed with DigitalMicrographs version 3.1 or higher. The optical density gradients in the background that are normally ramp-shaped were digitally corrected using a custom-made subroutine made compatible with DigitalMicrographs.

Shear Rheometry. Steady and small-amplitude oscillatory shear measurements were performed using a strain-controlled Rheometrics fluid spectrometer (RFS-II), which has a torque range of 0.002 to 100 g cm in two ranges with 1% accuracy. We used a standard Couette cell that contains the sample in a 1 mm concentric cylindrical gap between a cup (i.e., the outer cylinder) with a diameter of 34 mm and a bob (i.e., the inner cylinder) with a diameter of 32 mm and a length of 33 mm. About 12 mL of the sample is first loaded on the cup and fills the gap as the bob is lowered at a speed of 1 mm/s. All measurements were taken at 22 ± 0.5 $^{\circ}\text{C}$, and the temperature was controlled using a circulating ethylene glycol/water bath. To hinder water evaporation from the sample during the measurement, the relative humidity near the top air interface was kept near saturation by continuously purging water vapor through the sample surroundings using a humidifier. Also, the whole fixture assembly was covered with water-soaked foam-lined covers. The frequency dependences of storage and loss moduli (G' and G'') were measured for viscoelastic samples by linear dynamic (i.e., oscillatory) frequency sweeps from 0.05 to 100 rad/s at relatively small strain amplitudes, $\leq 25\%$. The linear regime (i.e., the region of low deformation where the rheological response is independent of the strain amplitude) was determined by dynamic strain sweep experiments. In nonlinear steady shear measurements with varying shear rates from 0.02 to 1000 s^{-1} , data were taken for both clockwise and counter-clockwise directions and averaged. Because of long transients at low shear in the viscoelastic samples, a preshearing delay of 120 s prior to an actual measurement was usually adopted for low shear rates, < 10 s^{-1} , and a 10 s delay was found to be enough at higher shear rates. The data presented in this paper were reproducible within an error limit of 5%.

Results

Micelle Morphology versus Molecular Composition. Aggregation morphologies formed at 23 $^{\circ}\text{C}$ in water by the di- and triblock copolymers (Table 2) were documented with cryo-TEM. Figure 1 first illustrates spherical micelles formed in a 1% aqueous solution of OB1. Fairly uniform dark spheres with an apparent diameter of 18 nm represent the PB micellar cores embedded in a light water matrix. The coronal domains where the hydrated PEO brushes are diffusively distributed provide a marginal contrast and appear as gray haloes surrounding the bright Fresnel fringes at this underfocus. As has been published elsewhere,³⁶ this interpretation has been shown to be essentially correct on the basis of through-focus serial imaging (not shown). For the copolymers used here, imaging micellar coronas was often possible (see Figure 8 for another example), and this unique observation of the corona domain that has never before been seen with other materials is perhaps connected to the fact

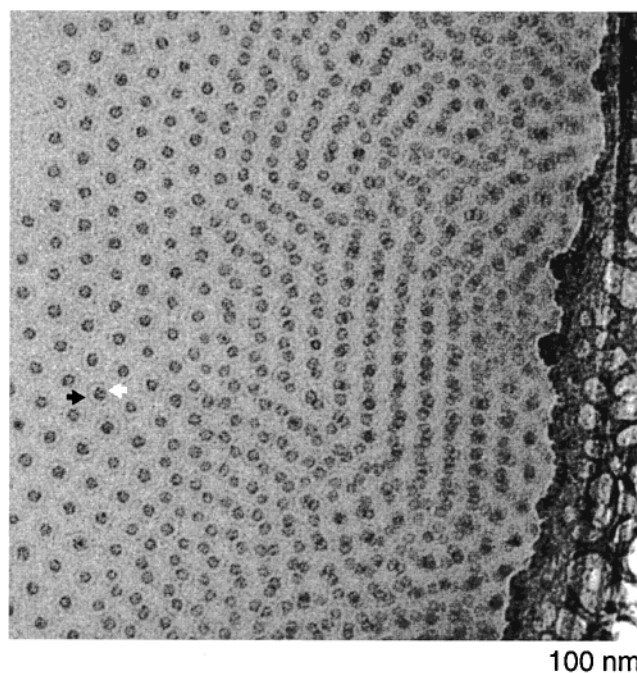
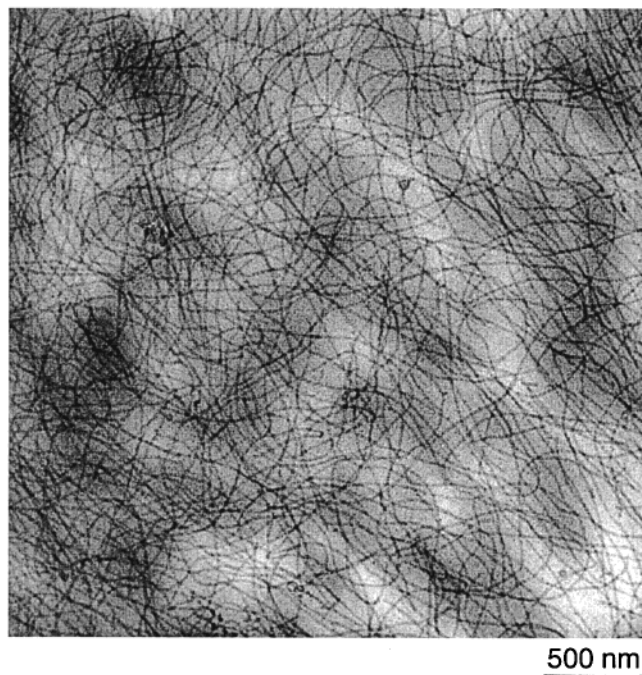


Figure 1. Cryo-TEM micrograph taken from 1% OB1 ($f_{\text{EO}} = 0.66$) in water. Uniformly sized spherical micelles were pushed toward the edge of the hole in the carbon–polymer layer. Partially shown in the right side of the image is the structure of the carbon–polymer film that was radiation-damaged by the electron beam. Not only the dark PB cores but also the gray haloes (filled arrow) representing the PEO corona domains were visualized. Fresnel fringe is indicated by the open arrow.

that the hydrophilic segment of PEO forms an unusual brush that is, despite favorable interactions with water molecules, significantly collapsed in the vicinity of the hydrophobic interface.³⁷ The freely suspended sample films usually assume a wedgelike shape, and such thickness variations in the specimens result in the nonuniform distribution of the micelles; that is, the micelles are concentrated around the edge of the sample film because the thickness is greater there than in the center.³⁸ Figure 1 illustrates a planar hexagonal packing of the spherical micelles driven by the size exclusion of the micelles from the center (e.g., top left corner) where presumably the film thickness is incompatible with the micellar size. Multiple layers are allowed to form at the edge, as evident in the image. The mean separation between the closely packed micelles is regarded as a characteristic micelle size representing the distance for hard sphere repulsive interactions and estimated to be approximately 43 nm.

By varying the PEO composition from 0.66 to 0.45, a micelle shape transition from spheres to cylinders was induced. Long entangled cylindrical (often referred to as *wormlike*, *threadlike*, or *polymer-like*) micelles with a cross-sectional diameter of 15 nm are displayed in the cryo-TEM image obtained for a 1% OB3 solution (Figure 2A). By tracing individual strands of the wormlike micelles, we can determine the value for micellar length that often exceeds 5 μm . Figure 2B taken at a higher magnification provides up-close nanostructural features such as spheroidal nubs and tips of the cylinders that have larger diameter and T-junctions. Branched wormlike micelles were first proposed by Porte et al. to explain anomalous rheological behaviors of cetylpyridinium chloride (CPCI) wormlike micelles in hexanol/water with excessive sodium chloride (NaCl)³⁹ and have been microscopically observed in not only mixed^{40,41,42} but also single-amphiphile⁴³ systems. Often it is difficult to clearly distinguish branches from overlaps because a TEM

A



B



Figure 2. Cryo-TEM images of 1% wormlike micelles of OB3 ($f_{EO} = 0.45$) at lower (A) and higher (B) magnifications.

micrograph merely provides a two-dimensional projection of a thin but still bulk specimen, and multiple imaging at different tilt angles is occasionally necessitated.⁴⁴ By contrast, the larger structures of polymeric micelles make the image interpretation straightforward. Branches are unambiguously distinguished from overlaps by measuring the optical densities at the junctions; that is, the overlaps appear darker than other parts of the micelles while the optical densities are uniform through the branches. Relevant examples are easily found throughout this paper.

Further decreasing the PEO composition produced membrane-like bilayers as evidenced in the images taken from a 1% OB2 solution (Figure 3). Vesicles (that is, curved, often closed

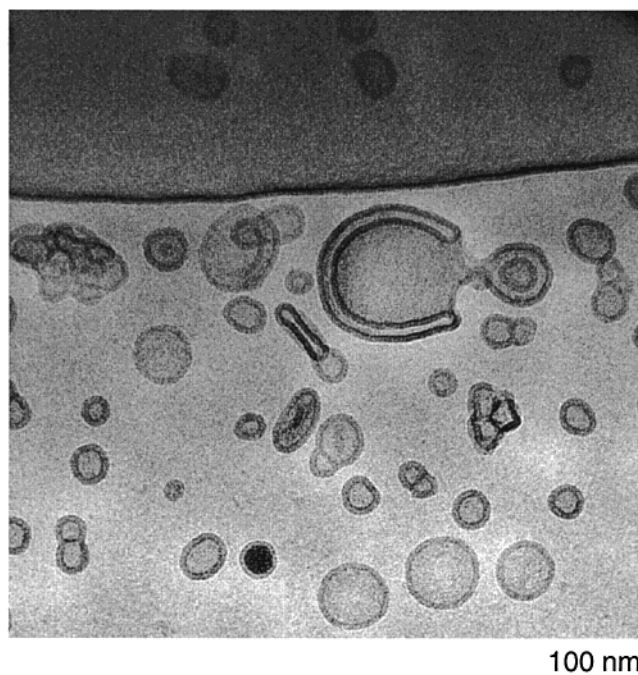


Figure 3. Cryo-TEM micrograph of vesicles formed by OB2 ($f_{EO} = 0.28$) at 1% in water.

bilayers encapsulating a fraction of the surrounding aqueous medium) made up of the copolymer are very diverse in size and shape. Here, we note that only the structures in a size range less than approximately 10^3 nm that can fit within the sample film were selectively visualized in the micrographs. Figure 3 partially displays a giant vesicle with a diameter of at least several micrometers, coexisting with complex small-sized (<300 nm) vesicles within and outside of itself. From the image, we estimated a fairly uniform bilayer thickness of 9 nm by tracing the density profile as a function of distance across the core domain. Here, it should be noted that, for vesicles, the core dimension was determined on the basis of the hypothesis that the projected core thickness has a sharp maximum at the inner surface and discontinuously drops to zero at the outer surface, and the inbetween portion is a parabolic-like decay.³⁵ Also seen is some roughness of the bilayers frozen presumably in the act of thermal undulation.⁴⁵ The sample also forms multilamellar vesicles and tightly packed monolayered vesicles appearing as foamlike structures.

The structures revealed by cryo-TEM are consistent with the results obtained from other measurements on the bulk samples such as visual observation and shear rheometry. Optical characteristics of the samples provide qualitative information on the dimensions of the colloidal domains. The 1% solutions of OB1 (spheres), OB3 (cylinders), and OB2 (vesicles) appear clear, bluish clear, and cloudy, respectively. The turbidity of the 1% OB2 solution in particular reflects the presence of particles with sizes comparable to the wavelength of light, as evidenced in the cryo-TEM micrographs.

The different morphologies were also investigated using rheological techniques. Viscosity measurements under steady shear from 0.02 to 1000 s^{-1} revealed that the solutions of OB1 (Figure 4A) and OB2 (Figure 4D) are Newtonian (that is, viscosity is independent of shear rate), while the OB3 solution exhibits a shear thinning (that is, the fall of viscosity with rising shear rate) (Figure 4B) with a power law of -0.82 for the shear rate dependence of the viscosity. This shear thinning behavior along with the elasticity exhibited at small deformation (that is, storage modulus $G' >$ loss modulus G'' at all measurement

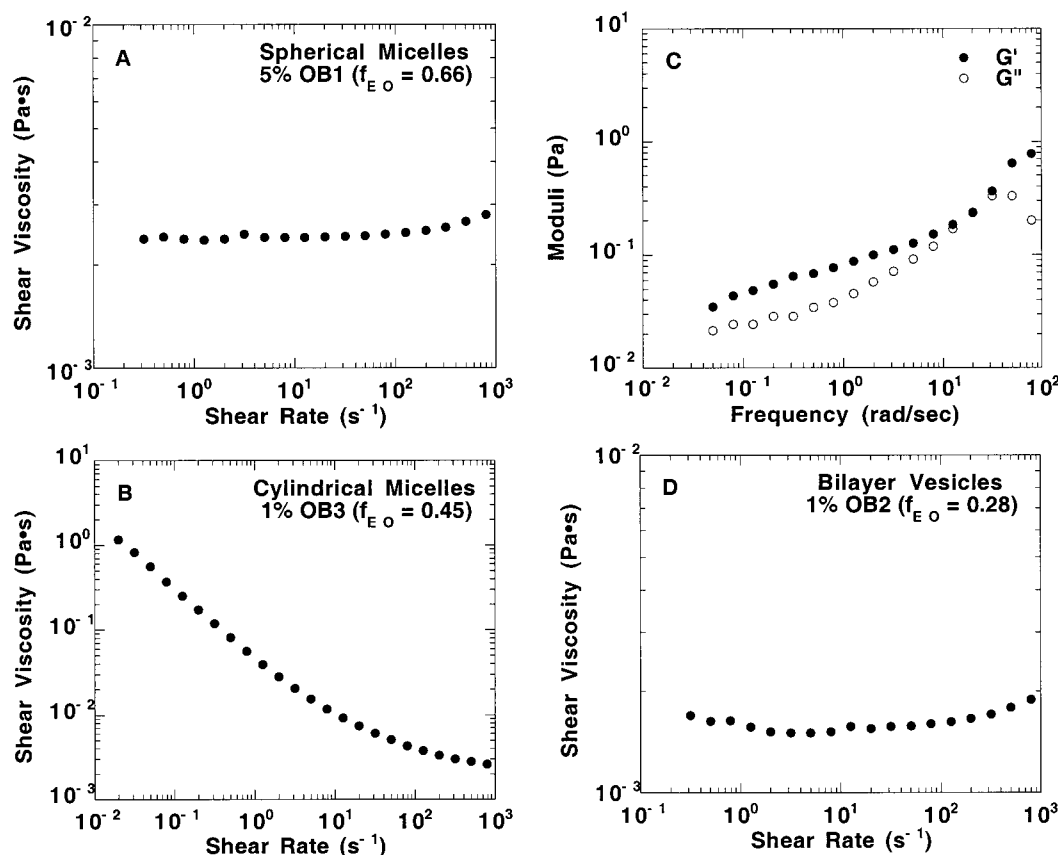


Figure 4. Rheological comparison of the three basic morphologies. The bulk rheological properties well agree with the structures directly visualized with cryo-TEM. The spheres of OB1 (A) and the vesicles of OB2 (D) exhibit the Newtonian-like behavior. The shearing thinning (B) and the linear elastic responses (C) of OB3 manifest the formation of polymer-like (i.e., long cylindrical) aggregates. A strain amplitude of 10% was employed to probe the frequency dependences of storage and loss moduli (G' and G'') of the 1% OB3 solution (C). The use of a higher concentration for the spherical micelles (A) was necessitated by the low-torque signal at lower concentrations.

frequencies) (Figure 4C) is in good agreement with the imaged long entangled wormlike micelles (Figure 2A). The use of a higher concentration (i.e., 5%) for the spherical micelles was necessitated by the low torque signal at lower concentrations, and a hydrodynamic micelle volume fraction of about 0.5 estimated from the measured shear viscosity is consistent with the overall micelle radius of about 43 nm obtained with cryo-TEM; see Figure 1. Prior studies of vesicles of small molecule surfactants such as AOT (sodium bisoctyl sulfosuccinate with NaCl) indicate that shear thinning and large elongation of the structure under shear can be traced to the large permeability of the membrane to water.⁴⁶ Therefore, the Newtonian response from the OB2 solution likely signals small deformations for the vesicles in shear flow and is consistent with the measured low permeability of the membrane to water ($\sim 2.5 \mu\text{m/s}$).⁴

Coexistence of Different Morphologies. A remarkable aspect disclosed by our cryogenic imaging of the polymeric aggregates is the coexistence of disparate morphologies for a single block copolymer. This behavior is normally found in two PEO composition ranges where the vesicle/cylinder and cylinder/sphere boundaries are located. Figure 5 presents an example where vesicles and wormlike micelles are found to coexist in a 1% solution of a PEO-PEE diblock copolymer OE7 ($f_{\text{EO}} = 0.39$). In this coexistence region, complex structures, particularly the fused threadlike micelle-vesicle compounds were frequently observed. The sample that the images were made of had been stored for one year after sample preparation, and no discernible disparity has been found in images taken from a sample two weeks after it had been prepared (not shown), indicating the long lifetime of such intermediate-like structures.

Very similar features were exhibited by a copolymer of a slightly higher $f_{\text{EO}} = 0.42$ (OE8) dissolved in excess water (i.e., 1%). The increased PEO composition is manifested in the dominance of wormlike micelles over vesicles as shown in Figure 6.

For $f_{\text{EO}} = 0.44$, a triblock PEO-PEE-PEO (OEO10) was examined. The 1% OEO10 solution provided a wide range of coexisting structures including unraveling threadlike micelle-vesicle hybrids, asterisk-shaped patches, flat bilayer fragments, looped and branched wormlike micelles, alveoli-like micelles, and unexpectedly, spheres in addition to cylindrical micelles and vesicles (Figure 7A-D). Wormlike micelles evolving from flat bilayer fragments at the edges have been previously documented for mixed ionic amphiphile systems and proposed as an intermediate structure appearing during lamella-to-cylinder transformation.⁴⁷ The micrographs taken at later time of the series of imaging (Figure 7A,C,D) contain the circular ringlike structures that are very faint in optical density compared to the bilayer structures, and we believe that they are cavities in the vitreous ice around the organic inclusions that have irreversibly formed after exposures of the sample to electron beam at the relatively high magnification.⁴⁸

Further increasing the PEO composition to $f_{\text{EO}} = 0.53$ resulted in pronounced micelle shortening (i.e., creation of more end caps and spheres) along with the disappearance of bilayers, as shown in Figure 8. The image shows resolved diffuse corona domains around the cylinders. The cryo-TEM imaging requires a considerable underfocus because of the low contrast between object and background, and this implies that there is a characteristic coronal dimension below which the corona

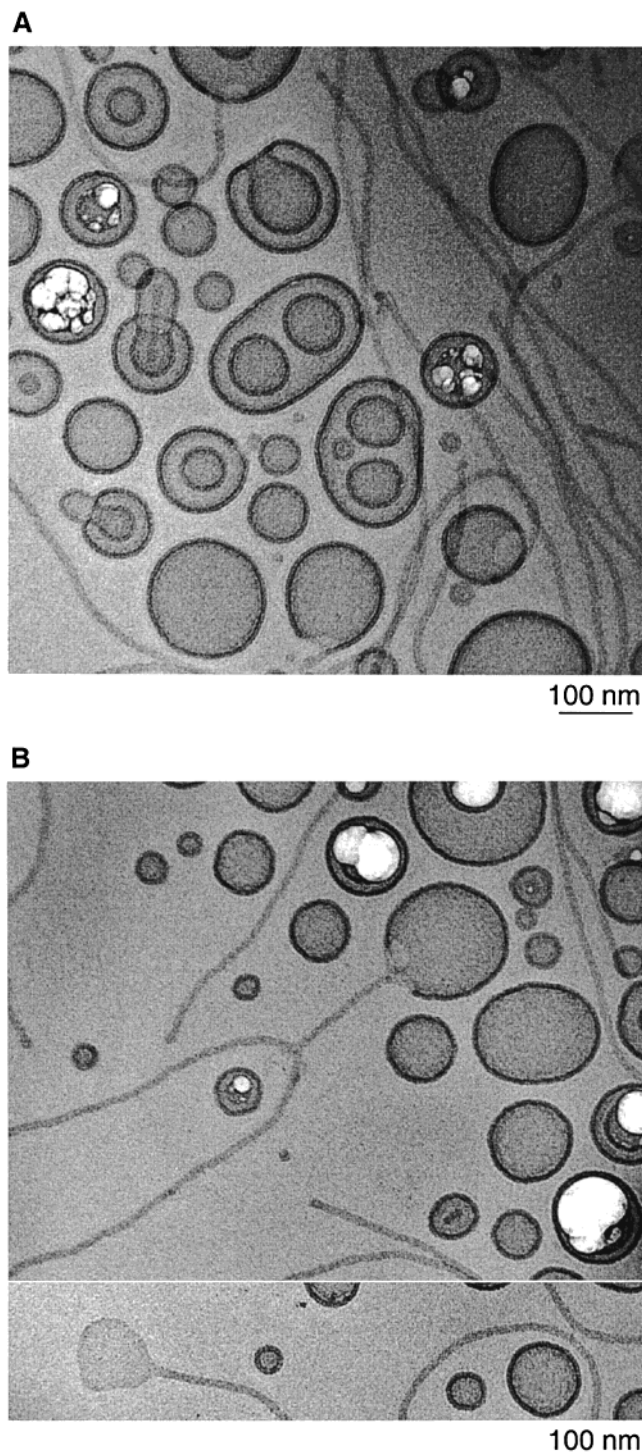


Figure 5. Coexisting vesicles and wormlike micelles formed by OE7 ($f_{EO} = 0.39$) at 1% in water. Vesicles are predominant over micelles. In panel A, the bright patterns are spongelike cavities formed during irradiation of the electron beam. In panels A and B, threadlike micelles growing from the edges of bilayers are ubiquitous.

visualization is prohibited by adjacent defocus effect (i.e., Fresnel fringe) caused by the core image. We found that the coronal domains are visible when the PEO micellar brushes are greater than roughly 5000 g/mol.

Independent studies of the sample using rheological techniques further support the images of shorter rods and spheres obtained for the 1% OEO1 solution and indicate that those structures are representative of the bulk sample in the cylinder-to-sphere region but not an artifact of the cryo-TEM instrumentation. Figure 9A,B present the linear and nonlinear

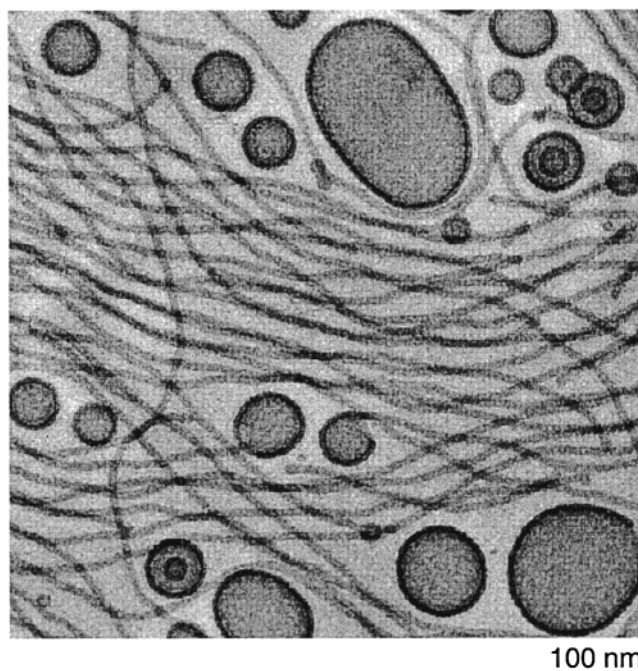


Figure 6. Cryo-TEM image obtained for a 1% OE8 ($f_{EO} = 0.42$) solution showing a coexistence between wormlike micelles and vesicles. There are more wormlike micelles than vesicles. Unraveling vesicles are also observed in the image.

rheological properties of a 1% OEO1 solution for a comparison to those for a 1% OEO10 solution (Figure 9C,D). The elastic responses at a small deformation and the shear thinning behavior under steady shear exhibited by the OEO10 ($f_{EO} = 0.44$) solution closely resemble those of OB3 ($f_{EO} = 0.45$) (Figure 4B,C). By contrast, the 1% OEO1 solution shows nonelastic (though not liquidlike) responses at a small deformation (i.e., loss modulus $G'' >$ storage modulus G' at all frequencies) and a very weak shear rate dependence of the viscosity under steady shear, which are intermediate to the behaviors of globular and entangled polymer-like micelles.

Figure 10 summarizes the overall structural behavior for the pure block copolymers as a function of the PEO volume fraction (f_{EO}). The sequence and ranges of the micellar shape transitions from bilayers to cylinders to spheres with increasing PEO composition were verified within the overall molecular weight range between 2.9 and 13.1 kg/mol.

Packing Properties of the Hydrophobic Segments. The high-resolution cryo-TEM measurements led to direct determination of the length scales of the core domains. The published value for the interaction parameter of $\chi_{PB/water} \approx 3.5$ (at 25 °C at low water content)⁴⁹ along with an estimate of $\chi_{PB/PEO} \approx 0.4$ at 25 °C (based on solubility parameters for the polymers estimated from group contribution calculations⁵⁰) indicates that the core materials are strongly segregated, and therefore, it is reasonable to assume that the core domain is effectively free of the other components (i.e., PEO and water). Further assuming the incompressibility of the core domain, it is possible to quantify the interfacial area per chain (a_o) from the measured core dimensions (R_c , that is the radius of the spheres or cylinders or half of the wall thickness for vesicles); the spread of the core dimension (R_c) normally has a standard deviation of 5–10% from the mean. Also, we introduce a dimensionless parameter s ($\equiv R_c/r_o$) taken as the ratio of the effective hydrophobic chain dimension normal to the hydrophilic–hydrophobic interface to their unperturbed end-to-end statistical length (r_o), representing a measure of the chain stretching that

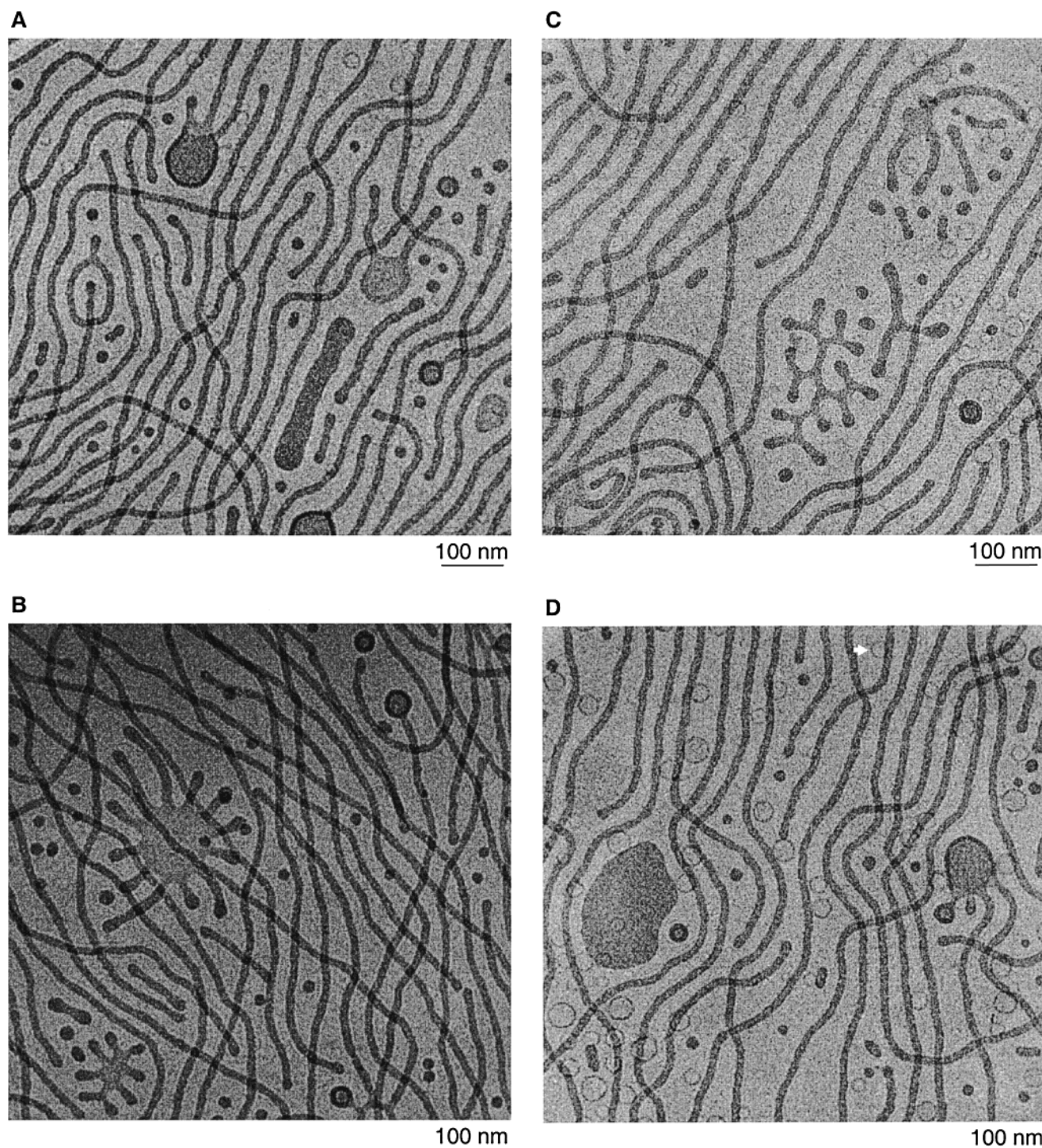


Figure 7. Cryo-TEM images from OEO10 ($f_{EO} = 0.44$). All three basic morphologies (i.e., bilayers, cylinders, and (unexpectedly) spheres) along with a spectrum of compound structures are displayed (panels A–D). The open arrow in panel D shows a pattern of electron beam damage, and the same was also seen in other micrographs (panels A and C).

presumably results from filling the corners of the unit molecular volume in the given geometries. In Table 1, we summarize the values of these parameters, R_c , a_o , and s , for the materials with 1,2-PB- or PEE-block sizes in a minimal range of $35 \leq N_{core} \leq 46$.

Figure 11 provides the correlation between the interfacial area per chain (a_o) and the degree of stretching (s) as functions of aggregation morphology. The ranges for individual morphologies in terms of the interfacial area are $1.0 \text{ nm}^2 \leq a_o \leq 1.1 \text{ nm}^2$ for bilayers, $1.2 \text{ nm}^2 \leq a_o \leq 1.5 \text{ nm}^2$ for cylinders, and $1.3 \text{ nm}^2 \leq a_o \leq 1.6 \text{ nm}^2$ for spheres. The interfacial area per chain, a_o , in general decreases with the changes in morphology from

spheres to cylinders to bilayers (as evidenced with OB1, OB2, and OB3, which are identical in PB molecular weight), and the significant overlap between spheres and cylinders is due to the values obtained for those coexisting in the triblock solutions (i.e., OEO1 and OEO10). When expressed in terms of the hydrophobic chain stretching, the regions characteristic for different types of aggregates do not overlap: that is, $1.0 \leq s \leq 1.2$ for bilayers, $1.6 \leq s \leq 2.0$ for cylinders, and $2.4 \leq s \leq 2.7$ for spheres. The chain stretching (s) lessens from spheres to cylinders to vesicles. Comparison of the three monodisperse PEO–PB diblocks (i.e., OB1, OB2, and OB3) that have the same PB length but only differ in PEO composition indeed

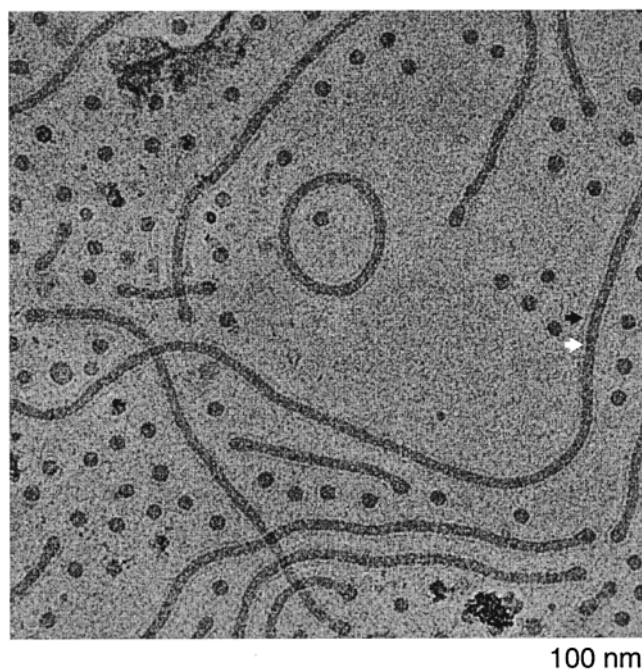


Figure 8. Cryo-TEM micrograph of short cylindrical micelles coexisting with spherical micelles obtained for OEO1 ($f_{EO} = 0.53$). Arrows are as in Figure 1.

illustrates that the PB core domains can be shaped and the dimensions adjusted to accommodate the variations in the hydrophilic volume per chain. We also note that for a given

choice of the micelle geometry the trend is obvious; a_0 decreases with increasing s .

Discussion

Cryo-TEM revealed the existence of several morphologies in dilute (i.e., 1 wt %) aqueous solutions of PEO-based di- and triblock copolymers (Table 2). The structural changes associated with variation of molecular composition resemble those previously documented for surfactants and lipids. Increasing the PEO composition (f_{EO}) causes a sequence of transitions from bilayers to cylinders to spheres, as anticipated by molecular-packing considerations.⁵¹ That is, interfacial curvature increases with increasing PEO composition to accommodate the increased asymmetry between hydrophilic and hydrophobic volumes per chain while respecting the constraints imposed by the connectivity between hydrophilic and hydrophobic blocks and the incompressibility of the core domain. The imaged structures correlate well with the observed macroscopic (i.e., optical and rheological) properties and therefore are considered to be representative of the bulk samples.

The correlation between the aggregate structure and the melt volume fraction of PEO (f_{EO}) summarized in Figure 10 is a result of the studies of the block copolymers in a molecular weight range between 2.9 and 13.1 kg/mol. It is reasonable to expect some molecular weight dependence to this correlation. The space filling of a flexible macromolecule is characterized by a power law, $R_g \sim N^\alpha$ where R_g is the radius of gyration and N is the number of repeat units. In melt state where polymer chains assume the form of random walk, the size (i.e., R_g) grows as a half power of their length (i.e., N),⁵² whereas the ~ 0.6 power

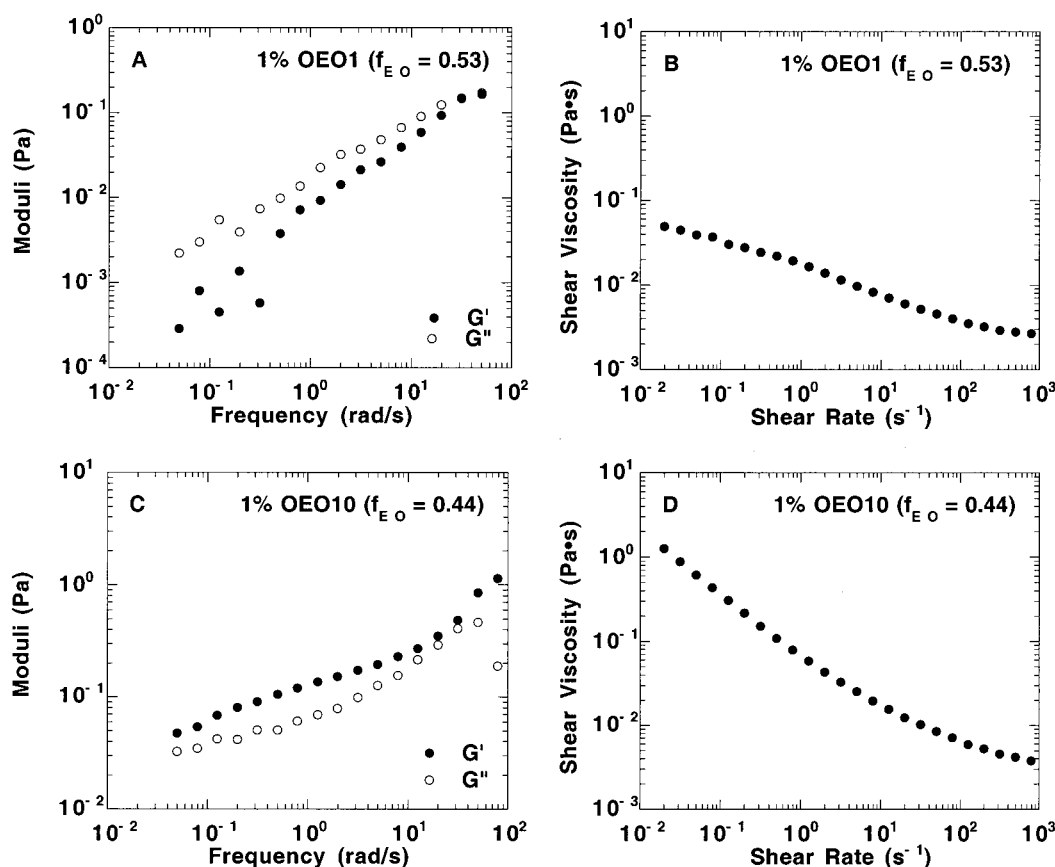


Figure 9. Macroscopic evidence for micelle shortening in terms of linear and nonlinear rheological behaviors. The frequency responses of 1% solutions of OEO1 (A) and OEO10 (C) were measured at strain amplitudes of 25% and 7%, respectively. Nonelastic behavior under small deformation and lower viscosity under steady shear exhibited by OEO1 are consistent with the decrease in micelle length evidenced in Figure 8. The rheological properties of OEO10 are quite comparable to those of OB3 (Figure 4).

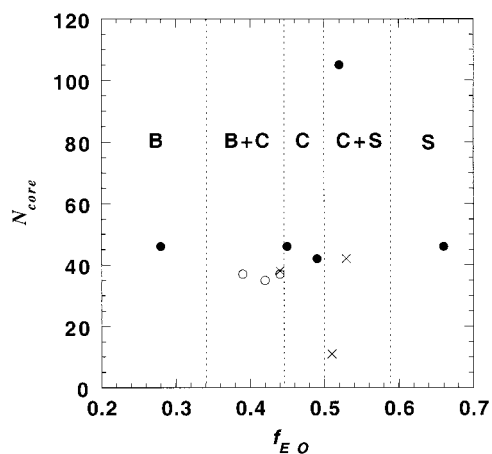


Figure 10. Experimentally determined correlation between the aggregation structure and the molecular composition. The observed basic aggregation geometries are bilayered lamellae (B), cylinders (C), and spheres (S). Coexistence behaviors were observed usually in two ranges between B and C or between C and S. The data points identify the PEO composition (i.e., f_{EO}) and the effective number of hydrophobic repeat units (i.e., $N_{PB} + 1$ or $N_{PEE} + 1$ for the diblocks, and $N_{PEE}/2$ for the triblocks); ●, ○, and × indicate PEO–PB, PEO–PEE, and PEO–PEE–PEO, respectively.

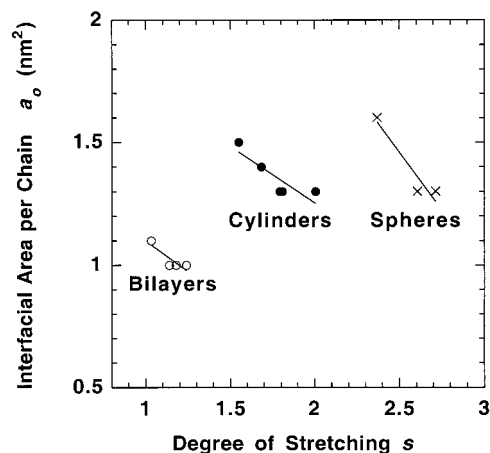


Figure 11. Correlation between the interfacial area per chain (a_o) and the degree of stretching (s) as a function of the aggregation structure: ○, ●, and × denote bilayer, cylinder, and sphere, respectively.

law characterizes the extended chains in a good solvent.⁵³ When neat or solvated macromolecules are attached to a surface by their ends (i.e., *polymer brushes*), the chain conformation is characterized by a new set of scaling exponents that are usually greater than that for the random walk configuration and apt to vary depending on the surface geometry and also the tethering density.⁵⁴ In general, the core and corona volumes scale differently with the chain length, and in fact, the corona domain likely has a stronger length dependence. For instance, on the basis of the scaling relations identified for the spherical starlike micelles,^{55–57} extending the overall size by a factor of n at a fixed composition will cause the increase of the core volume per chain by a factor of $n^{1.8}$ and the corona volume per chain by a factor between $n^{1.8-2.3}$. Therefore, qualitatively, it is expected that the bilayer-to-cylinder and cylinder-to-sphere boundaries will shift toward lower f_{EO} values when the overall molecular weight is increased at a fixed PEO composition. This structure–composition correlation in combination with the packing parameters (i.e., a_o and s ; see Table 1) provides an approximate a posteriori prescription for the packing properties of the polymeric amphiphiles in the dilute limit.

The mutually coexisting different-curvature structures exhibited by the single block copolymer solutions are a notable feature of the polymeric aggregates not expected from the previous studies of single-surfactant or single-lipid solutions. Experimentally, to claim equilibrium for such behavior requires us to show the path (i.e., sample history) and time independence of the observed behavior. Normally, no time dependence of the samples has been confirmed by the reproducibility of the micro- and macroscopic properties at different times over a year, indicating (erroneously we believe) equilibrium behavior. Alternatively, such morphological invariance could reflect long-lasting nonequilibrium states (see below).

In fact, such coexistence windows appear in two PEO composition ranges (i.e., $f_{EO} = 0.39-0.44$ and $0.51-0.53$) that are intermediate to the compositions for neat bilayers ($f_{EO} = 0.27$), neat cylinders ($f_{EO} = 0.45$), and neat spheres ($f_{EO} = 0.66$). One exception was found for the triblock copolymer OEO10 ($f_{EO} = 0.44$), which exhibits everything from spherical micelles to vesicles. In block copolymers, the composition domain is virtually continuous, and it is reasonable to expect that a few percentage points deviation in f_{EO} from an exact boundary may not completely suppress the metastability of the nonequilibrium structure. In a coexistence region, the difference between the chemical potentials of the block copolymer aggregate in the metastable (μ_m) and stable (μ_s) structures is perhaps $0 < \Delta\mu (= \mu_m - \mu_s) \ll k_B T$ (where k_B is Boltzmann's constant and T is temperature).

In this thermodynamic picture, the natural abundance of one structure relative to the other is a statistical reflection of the process of transitions between cylinders and bilayers achieved through synthetic adjustments of the hydrophilic content. At $f_{EO} = 0.42$ (OE8), wormlike micelles appear in excess over vesicles as shown in Figure 6, while slightly decreasing the volume fraction of PEO to $f_{EO} = 0.39$ (OE7) apparently yields the reverse (Figure 5). Intermediate structures such as the threadlike micelles welded to the vesicles at the edges are, however, commonly observed in both cases. It appears unlikely that such morphologies represent a captured transient state of, for instance, wormlike micelle formation by vesicle unraveling because they were invariably observed in a solution prepared years ahead (Figure 5). Recent freeze-drying TEM studies of the intermediates that form during the solvency-controlled vesicle-to-cylinder transition indicated that bowtie-shaped aggregates appear as a transient structure,⁵⁸ while paddle-shaped lamellae are recorded along the reverse structural pathway in solutions of PS–PAA with water and dioxane mixtures.⁵⁹ No evidence for such morphologies has been observed in any of our samples. As will be reported elsewhere,⁶⁰ the copolymers used in this study were found to exhibit no material exchange between the individual objects after formation at ambient temperature on the basis of quasi-static small-angle neutron scattering measurements, suggesting that the long-lived transient-like structures do not conform to the picture of intermicellar dynamic equilibrium.

One may argue that the polydispersity inherent in macromolecular samples is another factor that may at least partially contribute to the coexistence behavior. It is notable that, as shown in Figure 10, the relative volume fraction of hydrophilic block can change only by a few percentage, for example, to go from pure cylinders to their coexistence with spheres or bilayers, and this range of cylinder stability is comparable to the polydispersity of the copolymers (typically, around 10% in terms of the standard deviation in molecular weight distribution). The exact role of polydispersity in coexistence of micelle morphol-

ogies in equilibrium cannot, however, be established at present. Nonetheless, what seems most reasonable is that the coexistence behavior does not arise solely from polydispersity effects. Here, we note that anionically polymerized block copolymers having modest polydispersity typically produce highly regular and nearly monodisperse microdomains in the bulk state. The sphere/cylinder and cylinder/vesicle coexistence in two composition ranges demonstrated in our experimental phase diagram (Figure 10) bears a strong resemblance to that documented in a PS-PAA/dioxane/water system characterized by a block copolymer polydispersity of 1.05.⁶¹

A crucial insight is that slow kinetics associated with the high molecular masses may greatly hinder structural evolution toward global equilibrium after the genesis of the structure. Multiple mechanisms including unimer (i.e., single molecule of the amphiphile) exchange,⁶² fusion/fission of intermediate aggregates,⁶³ and even concerted cooperative association⁶² have been proposed for the equilibration of micelles in general. The dominant factor that controls the rate of component redistribution in any mechanism is the solubility of the amphiphilic molecules, that is, the tendency of the molecules to diffuse between domains separated by water, which is typically measured in terms of the critical micelle concentration (cmc). Previous studies of the nonionic surfactants between ethylene ($-\text{CH}_2-$) and ethylene oxide ($-\text{CH}_2-\text{CH}_2-\text{O}-$) oligomers suggest that the cmc drops exponentially with segment sizes.⁶⁴ Clearly, increasing the molecular weight over the nonionic surfactants will decrease the cmc dramatically; published values for the standard free energies of micelle formation per monomer ($\Delta G_{\text{mic}}(-\text{CH}_2-) = -1.15k_{\text{B}}T$ and $\Delta G_{\text{mic}}(-\text{CH}_2-\text{CH}_2-\text{O}-) = +0.32k_{\text{B}}T$ at 25 °C⁶⁴) reflect that micelles should form in extremely low concentrations for the copolymers, for instance, in the two morphology regions, and full hydration of such molecules seems simply impossible. As has been remarked, it is noteworthy that the individual objects formed in water by the block copolymers are practically isolated, and the coexistence most likely represents a nonequilibrium state; that is, the structure initially formed upon dissolution will likely be locked in.⁶⁰ Kinetic studies of thermodynamically perturbed micelles with small-molecule surfactants have identified a strong correlation between the molecular composition and the time scale for micelle redistribution.⁶² It is reasonable to expect that the kinetically restrained structures are most pronounced in vesicular systems where the amphiphiles have relatively low hydrophilic contents. In fact, we are aware of no thermodynamic model that accounts for the remarkable diversities in size and shape exhibited by the polymeric vesicles that have spontaneously formed without the considerable mechanical or chemical input and no previous reports of the formation of spontaneous vesicles of comparable nonuniformity (see Figure 3), and the results may thus only be understood as the effect of apparent absence of material exchange between discrete domains in vesicles.

Summary

This paper first examines the aggregation behavior of macromolecular surfactants such as PEO-PB, PEO-PEE, and PEO-PEE-PEO in the dilute limit, mainly as a function of the PEO composition. All of the basic aggregation geometries of membrane-like bilayer, cylinder, and sphere were identified for the pure materials with cryo-TEM, and a transition from low- to high-curvature structures could be induced by increasing the PEO composition. Not only the coexistence between the basic structures but also a vast array of long-lived intermediate and compound structures were evidenced in two ranges near

the bilayer-to-cylinder and cylinder-to-sphere boundaries, and such structural complexity in the single-amphiphile systems is largely attributed to the metastability rather than the polydispersity, both inherent in systems comprising polymeric materials. For the self-assembled structures that consist of the strongly amphiphilic block copolymers, the low tendency of molecular exchange between discrete domains (and therefore slow kinetics of the structural redistribution) may be another factor that suppresses the overall equilibration of the system. Validation and evaluation of these hypotheses are of continued research interest. Second, on the basis of quantitative structural measurements using cryo-TEM, we provide a phenomenological description of the packing properties of the amphiphilic polymers using parameters such as the interfacial area per chain (a_0) and the degree of hydrophobic chain stretching (s). For a given type of aggregate, the interfacial area per chain is inversely related to the hydrophobic stretching. As the structure is changed from bilayers to cylinders to spheres, both the interfacial area per chain and degree of hydrophobic chain stretching generally increase. When expressed in terms of the stretching degree, the ranges characteristic for individual structures are well apart, while there is a significant overlap between the spheres and cylinders in their interfacial areas per chain.

Acknowledgment. The authors thank Y. Talmon (Technion, Israel) and D. C. Morse (Minnesota) for many helpful discussions. Support for this research was derived from the University of Minnesota Materials Research Science and Engineering Center (MRSEC), a National Science Foundation (NSF)-sponsored research organization at the University of Minnesota.

References and Notes

- (1) Zhang, L.; Eisenberg, A. *Science* **1995**, 268, 1728.
- (2) Cornelissen, J. J. L. M.; Fischer, M.; Sommerdijk, N. A. J. M.; Nolte, R. J. M. *Science* **1998**, 280, 1427.
- (3) Won, Y.-Y.; Davis, H. T.; Bates, F. S. *Science* **1999**, 283, 960.
- (4) Discher, B. M.; Won, Y.-Y.; Ege, D. S.; Lee, J. C.-M.; Bates, F. S.; Discher, D. E.; Hammer, D. A. *Science* **1999**, 284, 1143.
- (5) *Vesicles*; Rosoff, M., Ed.; Marcel Dekker: New York, 1996.
- (6) Lu, B.; Li, X.; Scriven, L. E.; Davis, H. T.; Talmon, Y.; Zakin, J. L. *Langmuir* **1998**, 14, 8.
- (7) Tanford, C. *The Hydrophobic Effect*; Wiley: New York, 1973.
- (8) Israelachvili, J. N.; Mitchell, D. J.; Ninham, B. W. *J. Chem. Soc., Faraday Trans. 2* **1976**, 72, 1525.
- (9) Nagarajan, R.; Ruckenstein, E. *J. Colloid Interface Sci.* **1979**, 71, 580.
- (10) Nagarajan, R.; Ruckenstein, E. *Langmuir* **1991**, 7, 2934.
- (11) Puvvada, S. P.; Blankshtein, D. *J. Chem. Phys.* **1990**, 92, 3710.
- (12) Naor, A.; Puvvada, S.; Blankshtein, D. *J. Phys. Chem.* **1992**, 96, 7830.
- (13) Ben-Shaul, A.; Gelbart, W. M. In *Micelles, Membranes, Microemulsions, and Monolayers*; Gelbart, W. M., Ben-Shaul, A., Roux, D., Eds.; Springer: New York, 1994; p 1.
- (14) Alexander, S. *J. Phys. (Paris)* **1977**, 38, 983.
- (15) de Gennes, P.-G. *Macromolecules* **1980**, 13, 1069.
- (16) Dan, N.; Tirrell, M. *Macromolecules* **1992**, 25, 2890.
- (17) Wijnmans, C. M.; Zhulina, E. B. *Macromolecules* **1993**, 26, 7214.
- (18) Lin, E. K.; Gast, A. P. *Macromolecules* **1996**, 29, 390.
- (19) Milner, S. T.; Witten, T. A.; Cates, M. E. *Macromolecules* **1988**, 21, 2610.
- (20) Zhulina, E. B.; Borisov, O. V.; Priamitsyn, V. A. *J. Colloid Interface Sci.* **1990**, 137, 495.
- (21) Netz, R. B.; Schick, M. *Macromolecules* **1998**, 31, 5105.
- (22) Yu, K.; Eisenberg, A. *Macromolecules* **1996**, 29, 6359.
- (23) Yu, K.; Zhang, L. F.; Eisenberg, A. *Langmuir* **1996**, 12, 5980.
- (24) Yu, K.; Eisenberg, A. *Macromolecules* **1998**, 31, 3509.
- (25) Yu, K.; Bartels, C.; Eisenberg, A. *Macromolecules* **1998**, 31, 9399.
- (26) Zhang, L.; Yu, K.; Eisenberg, A. *Science* **1996**, 272, 1777.
- (27) Shen, H. W.; Zhang, L. F.; Eisenberg, A. *J. Phys. Chem. B* **1997**, 101, 4697.
- (28) Yu, K.; Zhang, L. F.; Eisenberg, A. *Langmuir* **1997**, 13, 2578.
- (29) Ferry, J. D. *Viscoelastic Properties of Polymers*; Wiley: New York, 1980.

- (30) Khandpur, A. K.; Macosko, C. W.; Bates, F. S. *J. Polym. Sci., Part B: Polym. Phys.* **1995**, *33*, 247.
- (31) Aharoni, S. M. *Macromolecules* **1983**, *16*, 1722.
- (32) Fetters, L. J.; Lohse, D. J.; Richter, D.; Witten, T. A.; Zirkel, A. *Macromolecules* **1994**, *27*, 4639.
- (33) Hillmyer, M. A.; Bates, F. S. *Macromolecules* **1996**, *29*, 6994.
- (34) Won, Y.-Y. Ph.D. Thesis, University of Minnesota, Minneapolis, Minnesota, 2000.
- (35) Bellare, J. R. Ph.D. Thesis, University of Minnesota, Minneapolis, Minnesota, 1988.
- (36) Zheng, Y.; Won, Y.-Y.; Bates, F. S.; Davis, H. T.; Scriven, L. E.; Talmon, Y. *J. Phys. Chem. B* **1999**, *103*, 10331.
- (37) Won, Y.-Y.; Davis, H. T.; Bates, F. S.; Agamalian, M.; Wignall, G. D. *J. Phys. Chem. B* **2000**, *104*, 7134.
- (38) Talmon, Y. *Ber. Bunsen-Ges. Phys. Chem.* **1996**, *100*, 364.
- (39) Porte, G.; Gomati, R.; El Haitamy, O.; Appell, J.; Marignan, J. *J. Phys. Chem.* **1986**, *90*, 5746.
- (40) Harwigsson, I.; Söderman, O.; Regev, O. *Langmuir* **1994**, *10*, 4731.
- (41) Lin, Z. *Langmuir* **1996**, *12*, 1729.
- (42) Silvander, M.; Karlsson, G.; Edwards, K. *J. Colloid Interface Sci.* **1996**, *179*, 104.
- (43) Danino, D.; Talmon, Y.; Levy, H.; Beinert, G.; Zana, R. *Science* **1995**, *269*, 1420.
- (44) Clausen, T. M.; Vinson, P. K.; Minter, J. R.; Davis, H. T.; Talmon, Y.; Miller, W. G. *J. Phys. Chem.* **1992**, *96*, 474.
- (45) *Structure and Dynamics of Membranes — From Cells to Vesicles*; Lipowsky, R., Sackmann, E., Eds.; Elsevier Science: Amsterdam, 1995.
- (46) Shahidzadeh, N.; Bonn, D.; Aquerre-Chariol, O.; Meunier, J. *Phys. Rev. Lett.* **1998**, *81*, 4268.
- (47) Walter, A.; Vinson, P. K.; Kaplun, A.; Talmon, Y. *Biophys. J.* **1991**, *60*, 1315.
- (48) Talmon, Y. In *Cryotechniques in Biological Electron Microscopy*; Steinbrecht, R. A., Zierold, K., Eds.; Springer-Verlag: Berlin, 1987; p 64.
- (49) *CRC Handbook of Polymer-Liquid Interaction Parameters and Solubility Parameters*; Barton, A. F. M., Ed.; CRC Press: Boston, MA, 1990.
- (50) van Krevelen, D. W.; Hoftyzer, P. J. *Properties of Polymers: Correlation with Chemical Structure*; Elsevier: New York, 1972.
- (51) Israelachvili, J. *Intermolecular and Surface Forces*, 2nd ed.; Academic Press: San Diego, CA, 1992.
- (52) Flory, P. J. *Principles of Polymer Chemistry*; Cornell University Press: Ithaca, NY, 1953.
- (53) de Gennes, P.-G. *Scaling Concepts in Polymer Physics*; Cornell University Press: Ithaca, NY, 1979.
- (54) Halperin, A.; Tirrell, M.; Lodge, T. P. *Adv. Polym. Sci.* **1992**, *100*, 31.
- (55) Halperin, A. *Macromolecules* **1987**, *20*, 2943.
- (56) Tao, J.; Stewart, S.; Liu, G.; Yang, M. *Macromolecules* **1997**, *30*, 2738.
- (57) Nguyen, D.; Williams, C. E.; Eisenberg, A. *Macromolecules* **1994**, *27*, 5090.
- (58) Burke, S. E.; Eisenberg, A. *Polymer* **2001**, *42*, 9111.
- (59) Chen, L.; Shen, H.; Eisenberg, A. *J. Phys. Chem. B* **1999**, *103*, 9488.
- (60) Won, Y.-Y.; Davis, H. T.; Bates, F. S. Unpublished work.
- (61) Shen, H.; Eisenberg, A. *J. Phys. Chem. B* **1999**, *103*, 9473.
- (62) Aniansson, E. A. G.; Wall, S. N.; Almgren, M.; Hoffmann, H.; Kielmann, J.; Ulbright, W.; Zana, R.; Lang, J.; Tondre, C. *J. Phys. Chem.* **1976**, *80*, 905.
- (63) Kahlweit, M. *J. Colloid Interface Sci.* **1982**, *90*, 92.
- (64) Meguro, K.; Ueno, M.; Esumi, K. In *Nonionic Surfactants: Physical Chemistry*; Schick, M. J., Ed.; Marcel Dekker: New York, 1987; p 109.